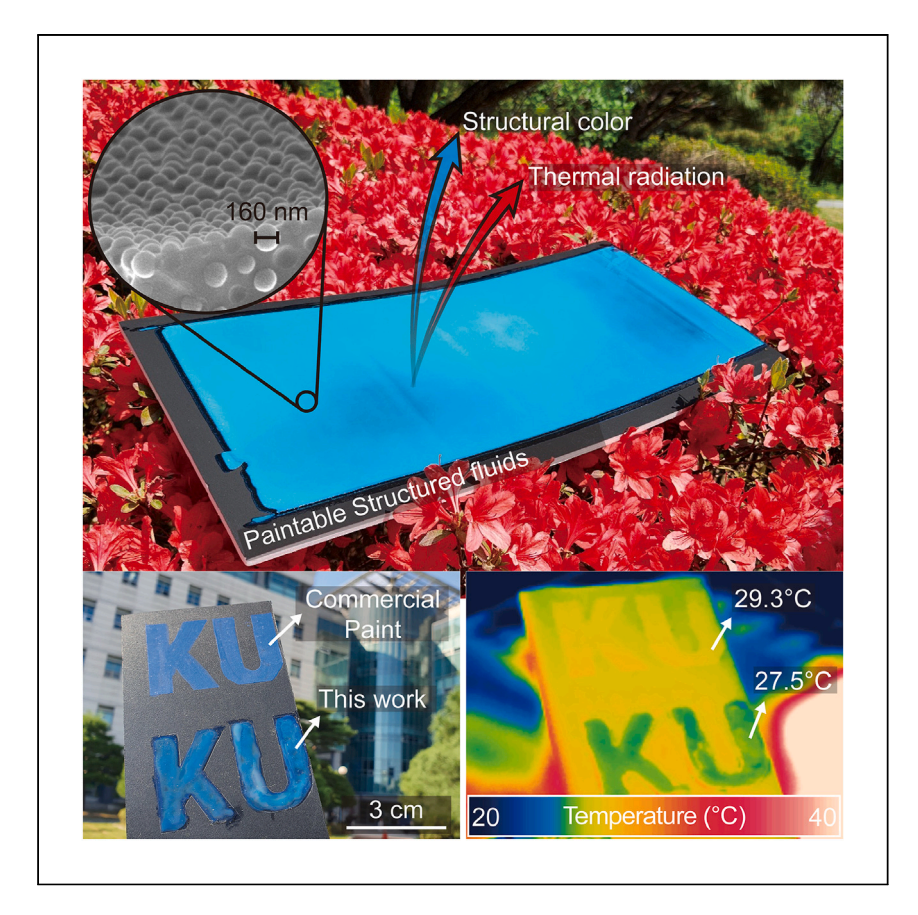


#### **Article**

# Structured fluids as colorful paintable radiative coolers



Kim et al. present the colorful radiative cooling paint (i.e., structured fluids) that simultaneously achieves low solar absorption ( $\approx$ 3%) and broadband high thermal emissivity (0.94). The structured fluids address the contradiction between effective cooling and colorization in daytime applications, highlighting the potential energy-saving benefits of radiative cooling.

Hyeon Ho Kim, Soyul Kwak, Jaewon Lee, Eunji Im, Aaswath P. Raman, Seungwoo Lee

seungwoo@korea.ac.kr

#### Highlights

The silica colloids with a polydispersity of  $\sim$ 0.1 present omnidirectional color

The structured fluids present a 3% solar absorption and an IR emissivity of 0.94

The structured fluids serve as a radiative cooling paint covering large areas

The IR emissivity and cooling performance are improved by soft imprinting

Kim et al., Cell Reports Physical Science 5, 102068

July 17, 2024 © 2024 The Authors. Published by

https://doi.org/10.1016/j.xcrp.2024.102068





#### **Article**

## Structured fluids as colorful paintable radiative coolers

Hyeon Ho Kim, <sup>1</sup> Soyul Kwak, <sup>1</sup> Jaewon Lee, <sup>1</sup> Eunji Im, <sup>2</sup> Aaswath P. Raman, <sup>3</sup> and Seungwoo Lee<sup>1,2,4,5,6,\*</sup>

#### **SUMMARY**

Radiative cooling has emerged as a promising materials-driven approach to enabling passive cooling for terrestrial structures. The prevalent wavelength-selective, solar absorption-driven colorization strategies have hindered cooling performances, especially during the daytime. In this study, we present a structured fluids platform that can simultaneously achieve extremely low absorption across the solar spectrum (≈3%) and preservation of omnidirectional, full-color characteristics. In addition, it serves as an ideal broadband emitter in the infrared (IR) range, with an emissivity of up to 0.94. This enables sub-ambient (~2 K) daytime radiative cooling with a power of ~40 W/m<sup>2</sup> on a reflective substrate. In addition, on an absorptive substrate, the structured fluids effectively cool the substrate by up to 9.5 K with a power of  $\sim$ 120 W/m<sup>2</sup>. Furthermore, the exotic fluidity of structured fluids facilitates compatibility with scalable painting and molding, offering versatile and efficient solutions for sustainable energy-saving cooling applications beyond conventional radiative methods.

#### INTRODUCTION

Since the translation of initially nighttime-limited radiative coolers into a daytimeworking regime through thermal nanophotonics in 2014,<sup>1</sup> the field of radiative cooling has experienced a significant surge in interest from diverse research communities due to its potential to mitigate global warming without additional energy consumption.<sup>2</sup> While the original demonstration of daytime radiative cooling involved reflective and later white surfaces, researchers have since pursued the colorization of radiative coolers, 3-18 recognizing that meeting aesthetically demanding criteria could accelerate the widespread adoption of radiative coolers for immediate practical applications, such as building-, 9,11,12,14-16,19-22 automobile-, 9,11,12,14,15 and cloth-integrated cooling systems. <sup>6,7,17,23,24</sup> Recent work compared the cooling performances of two structurally different radiative emitters—those with identical color appearance but different absorption spectra over the visible regime (known as metamerism).<sup>5</sup> It turned out that minimizing absorption has been shown to be critical to enabling efficient daytime radiative cooling (Figure 1A) because increased solar absorption inevitably raises the temperatures of emitters. We theoretically reproduced this importance of non-absorbing colorization particularly for daytime radiative cooling of the selective and non-selective emitters, as shown in Figure 1B (also see Figure S1). Without solar absorption, the selective emitter can exhibit a lower equilibrium temperature than its non-selective counterpart because non-selective emitters absorb more downward thermal radiation from the atmosphere than selective emitters.<sup>25</sup> More important, it is worth noting that the equilibrium temperatures of both emitters increase with a higher solar absorption; the selective emitters show a steeper slope of this increase in temperature than the non-selective counterpart.

<sup>1</sup>KU-KIST Graduate School of Converging Science and Technology, Korea University, Seoul 02841, Republic of Korea

<sup>2</sup>Department of Biomicrosystem Technology, Korea University, Seoul 02841, Republic of Korea

<sup>3</sup>Department of Materials Science and Engineering, University of California, Los Angeles, Los Angeles, CA 90095, USA

<sup>4</sup>Department of Integrative Energy Engineering (College of Engineering) and KU Photonics Center, Korea University, Seoul 02841, Republic of Korea

<sup>5</sup>Center for Opto-Electronic Materials and Devices, Post-Silicon Semiconductor Institute, Korea Institute of Science and Technology (KIST), Seoul 02792, Republic of Korea

<sup>6</sup>Lead contact

\*Correspondence: seungwoo@korea.ac.kr https://doi.org/10.1016/j.xcrp.2024.102068





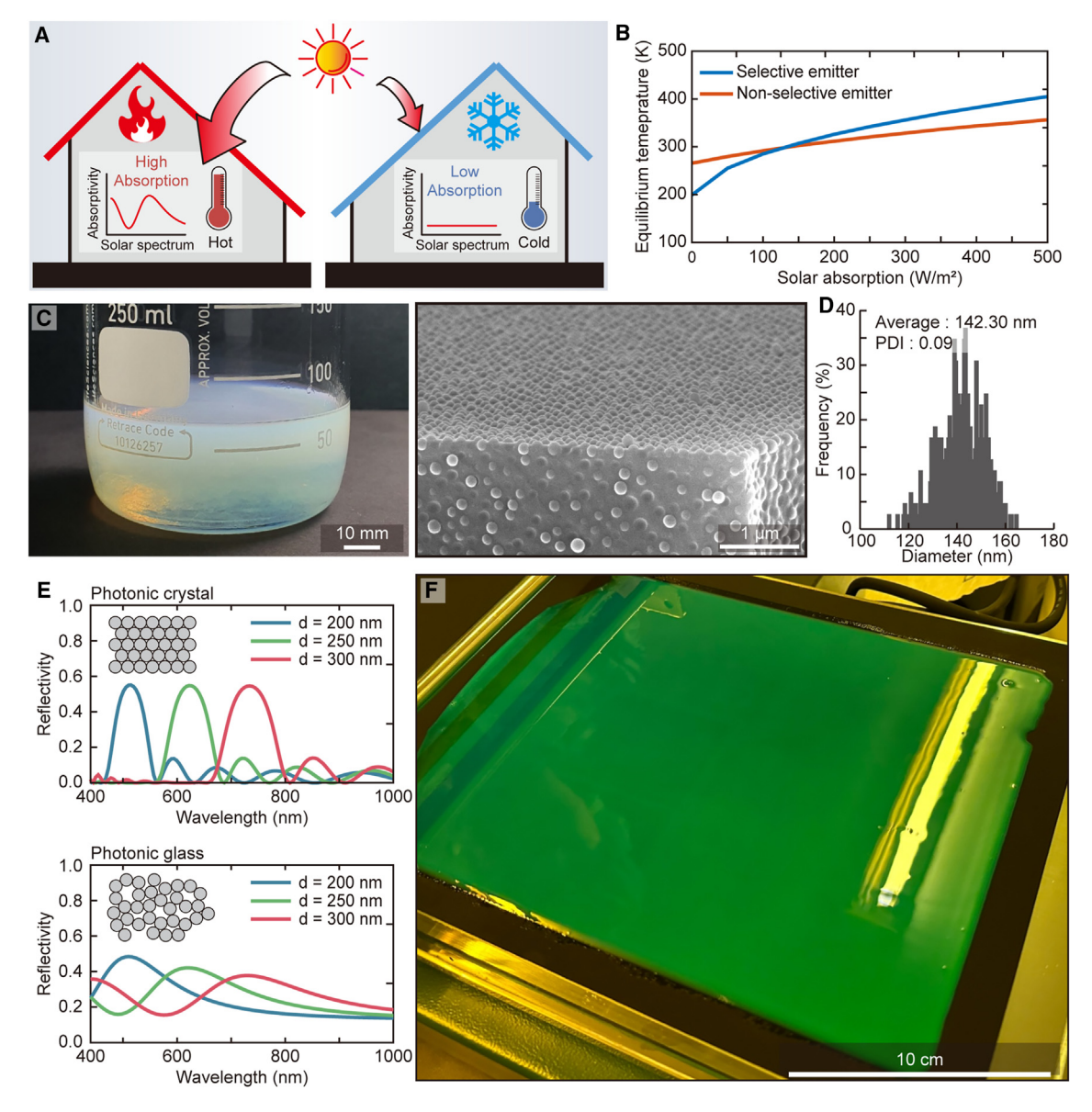


Figure 1. Colloidal photonic assemblies for colorful cooling paint

(A and B) Schematic (A) and graph (B) illustrating the relationship between solar absorption and temperature. Regardless of the thermal emitter type, lower solar absorption is a crucial factor in promoting daytime radiative cooling.

- (C) Macroscopic image of the liquid-phase structured fluids (left) and microscopic image (SEM) of the robustly cured structured fluids (right).
- (D) Statistical data for the size distribution of silica colloids corresponding to (C). The average diameter, SD, and PDI of the silica colloids are 142.03 nm, 13.73 nm, and 0.09, respectively.
- (E) Reflectivity spectra of the PhCs (top) and photonic glasses (bottom) composed of 200-, 250-, and 300-nm-size silica colloids, respectively.
- (F) Bird's-eye view of the large-scale area (150 imes 150 mm) coated with the structured fluids by doctor blading.

This is because the cooling power of the non-selective emitter can be higher than that of selective emitters.  $^{25}$ 

Despite this straightforward blueprint, the prevailing strategy for color preservation in radiative coolers has still depended on solar absorption at specific visible wavelengths, resulting in less-efficient cooling power than traditional whitish counterparts. 3-7,9,13,15-18 Exceptionally, reflection- and scattering-based colorization methods, including stacked dielectric Bragg reflectors, 5,8,14 droplet-based total

#### Article



internal reflectors (TIRs), <sup>12</sup> and particular scatters, <sup>10,11</sup> have been implemented into colorful radiative coolers. However, these diffractive and TIR reflectors suffer from incident angle-dependent colorization, and more critically, their absorptions in the visible regime have not been negligible. Deposition-type diffractive coolers, relying on state-of-art infrastructures (e.g., vacuum-based deposition facilities), are challenging to cost-effectively translate into practical applications requiring scalability, such as building-integrated radiative coolers. Soft self-assembly methods, such as 1D cellulose Bragg stacks, TIR droplets, and particular scatters, offer otherwise impossible easy accessibility for scalable applications like simple painting. However, the intrinsic instability of these soft assemblies makes them less robust against external mechanical deformations and requires highly trained personnel, rendering them impractical for commodity usage, especially in outdoor environments.

In this work, we introduce structured fluids<sup>26,27</sup> as paintable, robust, and full-colored radiative coolers, simultaneously addressing ultralow solar absorption and ideal broadband thermal radiation. Figure 1C shows macroscopic (bird's-eye view) and microscopic (scanning electron microscopy [SEM]) images of a liquid phase and robustly cured structured fluids (continuous film), respectively, where 120- to 175-nm silica colloids are disordered within the trimethylolpropane ethoxylate triacrylate (ETPTA) matrix (i.e., photonic glass film). In the visible spectrum, these structured fluids exhibit consistent colorization regardless of the viewing angle, which is attributed to resonant light transport of photonic glass.<sup>28-33</sup> Simultaneously, the strong molecular vibrations of silica and ETPTA transform structured fluids into a bulk homogeneous radiative medium at the mid-infrared (mid-IR) regime, efficiently dissipating broadband thermal loads into outer space.<sup>8,34–36</sup> Moreover, owing to their soft fluidity, versatile brush painting or bar coating enables large-scale fabrication of structured fluids onto demanding objects; subsequent thermal and photonic treatments can solidify the coated fluids into a mechanically robust film. <sup>37–39</sup> Overall, our structured fluids provide a versatile material platform for full-color radiative cooling paints as with the commercial acrylic resin-based paints, 40,41 simultaneously addressing scalability, robustness, and low solar absorption—challenges that were difficult to overcome with other platforms.

#### **RESULTS AND DISCUSSION**

#### Colloidal photonic assemblies

In previously reported silica/ETPTA photonic crystals (PhCs), the use of the monodispersed colloids was the key to achieving entropic crystallization. 42-47 By contrast, to develop our structured fluidic coolers, we used the polydispersed silica colloids with a polydispersity index (PDI) of 0.09 (Figure 1D; see also Figure S2). Since the dielectric constants of silica and ETPTA retain almost identical values (Figure S3), 41,42 the attractive enthalpy between the monodispersed silica colloids (e.g., van der Waals forces) could be effectively reduced within the ETPTA host medium. Thus, with an increase in volume percent (vol %) of the silica colloids in ETPTA monomeric fluids, a repulsive entropic crystallization of colloids emerged (i.e., silica opals in ETPTA). However, encoding a moderate PDI of 0.09 to silica colloids facilitated their random organization in ETPTA monomeric fluids (Figures 1C and 1D), while maintaining a short-range order akin to other colloidal photonic glasses. <sup>28–33</sup> Since the size distribution of the silica colloids was still narrow, these photonic glasses enabled resonant light scattering. This involves scattering from randomly distributed individual colloids (form factor) and subsequent resonant light diffusion along the short-range order of colloids (structural factor). <sup>29–33</sup> Consequently, the structured fluids achieved isotropic scattering and the resultant omnidirectional colorization with negligible



solar absorption, starkly contrasting with the typical silica opals in ETPTA (Figure S4).  $^{42-47}$  Additionally, the interplay between form and structural factors in photonic glass can yield a broader spectral scattering than the diffractive scattering of PhCs. Figure 1E contrasts the reflectivity spectra between PhCs (top) and photonic glasses (bottom) composed of 200-, 250-, and 300-nm silica colloids, respectively. Here, regardless of the colloid sizes, PhC and photonic glass, each with a thickness of 2  $\mu$ m, are assumed to be filled with 74 and 50 vol % of silica colloids, respectively. Photonic glasses can reflect more solar light than PhCs, even with the lower vol % of silica colloid, as they can more broadly reflect the incoming solar spectrum. As such, photonic glasses were found to be advantageous over PhCs in daytime radiative cooling (see the detailed optical and thermal comparison between PhCs and glasses in Figure S5).

More critically, this underpinning mechanism of structured fluids ensured robust colorization during the painting process. Traditional painting methods, such as brush painting and bar coating, are prone to a shear thinning of fluids, potentially elongating colloidal distance in a fluidic face-centered-cubic (FCC) crystal and differentiating the resulting diffractive colorization. In contrast, the colorization of fluidic photonic glass relies primarily on individual particle scatterings and resonant diffusions of the scattered light, as mentioned above. Thus, given the vol %, the size of silica colloids becomes the main determinant for defining the available colors from photonic glass fluids, rendering the colorization of our structured fluids resistant to the personnel-dependent painting processes. A representative example is shown in Figure 1F, where structured fluids coated over a large area (150 × 150 mm) by doctor blading (i.e., 175-nm silica colloids with 27 vol %) exhibits omnidirectional and consistent color.

#### **Optical properties**

Control over the size and vol % of silica colloids enables the realization of full-color structured fluids. Beyond the aforementioned greenish fluids, we developed bluish (B) and reddish (R) fluids using 120-nm colloids with 20 vol % and 160-nm colloids with 15 vol %, respectively. The vol% of the silica colloids (i.e., 15-30 vol %) to present desired colors through resonant scattering was empirically determined. These RGB (red, green, blue) fluids, each with a thickness of 300 µm, were capillary coated onto Si substrates using a glass plate and spacer, followed by curing through UV light illumination (Figure 2A). The SEM images and corresponding fast Fourier transform (FFT) images of the top surface of each cured film are presented in Figure 2B (from left to right, corresponding to B, G, and R). Statistically quantifying the probability of colloidal distances, as shown in Figure S6 (i.e., radial distribution function analyses for centroid-to-centroid distribution of colloids), revealed no correlation between the long-range colloidal distances. This confirmed a random organization of silica colloids within the ETPTA matrix. However, a distinct peak at the shortest distance between colloids remained evident across the RGB fluids, indicating the presence of short-range order. Therefore, we anticipate the interplay between form and structural factors in terms of the resonantly diffusive colorization from these structured fluids.

To quantify the diffusive colorization more precisely, we conducted experimental and theoretical analyses on the three different color films (Figures 2C, 2D, S7, and S8). The numerically calculated reflection spectra (Figure 2C) for the three different color films agreed well with the experimental results (Figure 2D), confirming the accurate reproduction of the structured fluids by the calculation model. Modal analyses of the films (Figure S8) indicated that the structured fluids scatter light



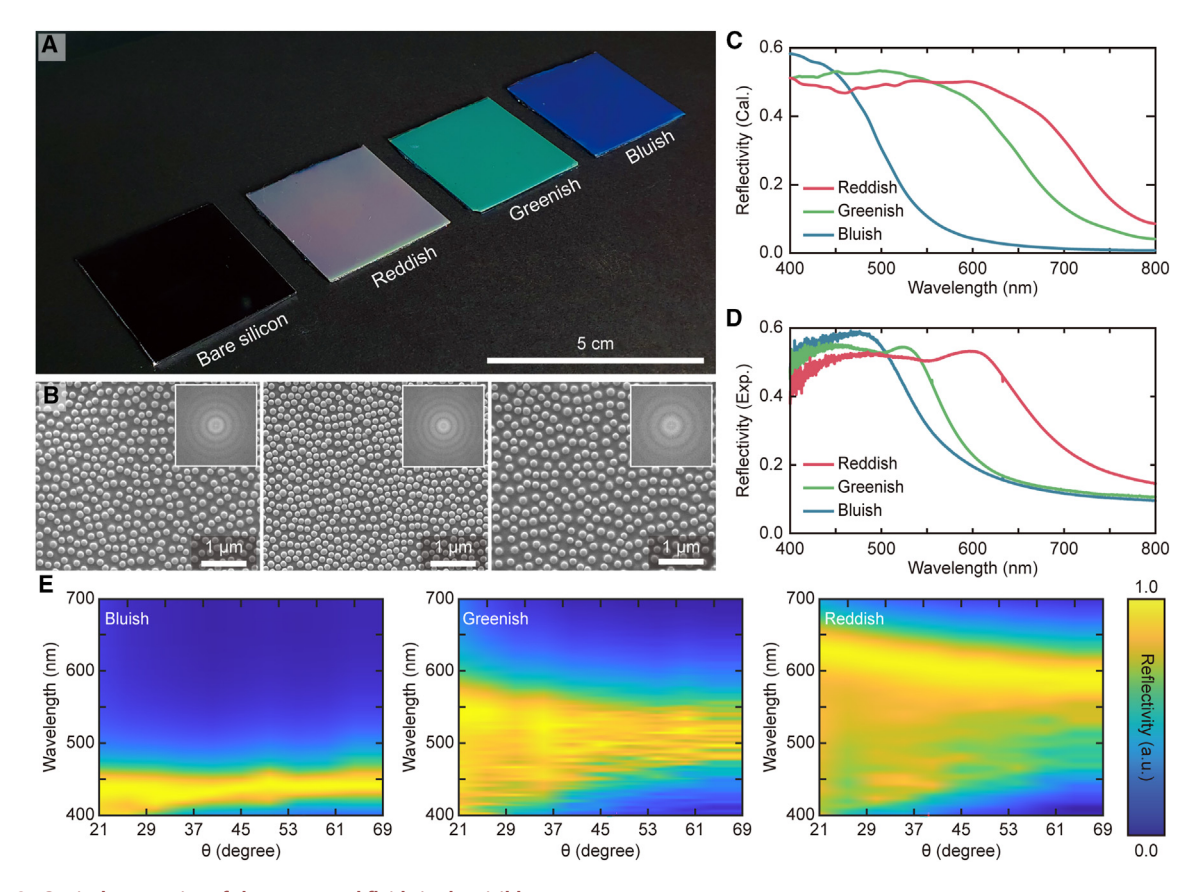


Figure 2. Optical properties of the structured fluids in the visible range

(A) Bird's-eye view of the RGB structured fluids films (i.e., photonic glass films) coated on the Si substrate, with a thickness of 300  $\mu$ m. (B) SEM images and FFT images (inset) of the structured fluids films corresponding to (A). From left to right, each image represents the B, G, and R films, respectively.

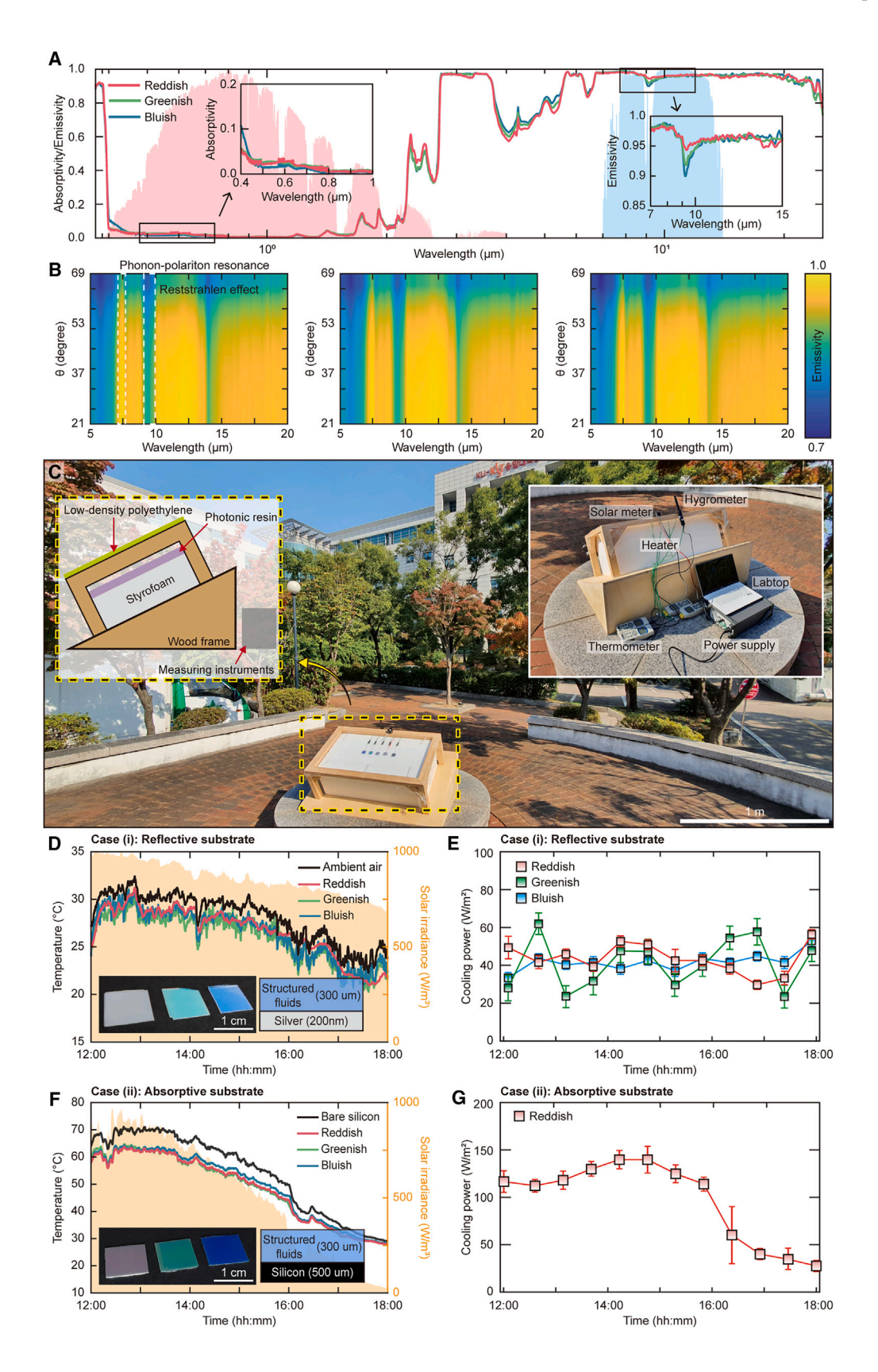
(C and D) Numerically calculated (C) and experimentally measured (D) reflection spectra of the 3 different colors of structured fluids films. The spectral peaks in (C) coincide with the reflective peaks in (D).

(E) Angle-resolved reflection spectra of the B, G, and R films (left to right). Since the short-range order scatters the longer wavelength, the reflection spectra become broader from B to R.

diffusively, as evidenced by randomly distributed scattered electric fields. Moreover, as shown in Figures 2C and 2D, the broad reflection across the visible range and two spectral peaks in the reflection spectrum (G and R fluids) further support the diffusive light scattering of the structured fluids. In detail, the G and R fluids showed nearly identical scattering wavelengths below 500 nm, as the scattering from individual colloids (Mie scattering) at the given particle size (i.e., 160–175 nm) remained consistent, as presented in Figure 2D. In contrast, the wavelengths of the structural factor-driven scattering, differentiated by their short-range orders, ranged from 480 to 620 nm. Notably, 175-nm and 160-nm silica colloids with the vol % of 0.27 and 0.15 led to scatterings at 530 and 620 nm wavelengths, respectively. Given the form factor-relevant background scattering in the bluish regime (450–480 nm), these structural factor-driven scatterings resulted in the color appearance of G and R, respectively. For the B fluid film, composed of 120-nm silica colloids, its form factor spectrally reflected the ultraviolet (UV) regime because of particle size; therefore, only the structural factor governed the appearance of the B color.<sup>30</sup>

Resulting from the isotropy of diffusive scattering, our structured fluids films (photonic glasses) indeed showed consistent colorization regardless of view angles, as





#### **Article**



#### Figure 3. Thermal properties of the structured fluids

(A) Absorptivity/emissivity of the three different structured fluids films from 200 nm to 20  $\mu m.$ 

(B) Angle-resolved emissivity spectra of the B, G, and R films (from left to right). Phonon-polariton resonance and the reststrahlen effect modes are highlighted in a white dotted box.

(C) Bird's-eye view of the outdoor experiment location (37°35′24.0″N 127°01′36.4″E). Two experimental cases (i.e., structured fluids with reflective substrate and absorptive substrate) were conducted for the outdoor experiments.

(D–G) Time-traced outdoor daytime radiative cooling performance of the structured fluids with (D and E) reflective substrate and (F and G) absorptive substrate. (D) Temperature variation of the reddish, greenish, and bluish structured fluids films on an Ag substrate and solar irradiation measured on March 14, 2024. (E) Time-traced cooling powers variations on March 18, 20, and 21, 2024, for reddish, greenish, and bluish, respectively. Data are represented as average  $\pm$  SD. (F) Temperature variation of the structured fluids films on a Si wafer and solar irradiation measured on June 22, 2022. (G) Time-traced cooling power variation corresponding to (F). As a representative case study, the cooling power of the R film was measured. Data are represented as average  $\pm$  SD.

shown in the bird's-eye view of B film (Figure S9) and angle-resolved reflection spectra of the RGB films (Figure 2E, B, G, and R film image from left to right). From B to R, the short-range order (structural factor) scattered longer wavelengths, resulting from a wider spacing between particles (e.g., lower vol % at a given particle size). In contrast, scattering from a single particle (form factor) remained consistent regardless of the vol %. This results in broader angle-resolved reflection spectra as the form and structural factors were spectrally detached, as shown in Figure 2E. As mentioned in Figure S5, the spectrally broadband scattering of the visible regime can be advantageous for daytime radiative cooling, even if it compromises color purity (Figure 2A).

#### Thermal properties

Next, we characterized the absorptivity/emissivity of the RGB-structured fluids films, as shown in Figure 3A. Since both materials (i.e., silica colloids and ETPTA matrix) are intrinsically transparent in the solar spectrum (Figure S3), the structured fluids films barely absorbed solar energy (≈3% at 200-4,000 nm). The light, neither reflected nor absorbed, readily passes through the structured fluids films, enabling their application as transparent radiative coolers. 48 Therefore, as in many other previously reported papers, the transmitted light can be absorbed by an underlying absorptive substrate (e.g., Si wafer), 5,8,13 whereas a reflective substrate (e.g., silver [Ag] mirror) can reflect the incoming broadband solar light back to outer space. 10-12,14,15 In the mid-IR regime, the structured fluids can be transformed into a deep-sub-wavelength-scale bulk thermal emitter, as the colloidal size was too small to interact with the mid-IR range electromagnetic waves. Benefiting from the molecular vibrations of the silica colloids and ETPTA matrix, the structured fluids can dissipate thermal energy as a broadband emitter (0.94 emissivity from 5- to 20-μm wavelengths), regardless of color (Figures S10A and S10B). Despite the spectral dip of absorptivity at a 9.3-µm wavelength (right inset image of Figure 3A), originating from the reststrahlen effect (i.e., impedance mismatch), 1,11,49 our works achieved remarkable thermal emissivity ( $\approx$  0.96) at the transparent window range. These properties arise from the interplay between the phonon-polariton resonance mode of the silica colloid  $^{1,11,49}$  and the bulk emission from the thick emitter ( $\sim 300 \, \mu m$  thick).  $^{8,34,35}$ As a result, the structured fluids films simultaneously can achieve lower solar absorption and higher thermal emission than other colorful radiative coolers (see Figures S10C and S10D). 8,10-14,50 Figure 3B shows the angle-resolved emissivity spectrum of the B, G, and R structured fluids films from left to right, respectively. Since the structured fluids are effective homogeneous media in the mid-IR regime (Figure 3B), the phonon-polariton resonances and reststrahlen effect modes were observed regardless of view angles, colloidal size, and vol %.

The combination of low solar absorption in the visible regime and high thermal emission in the mid-IR regime resulted in outstanding daytime radiative cooling



performance. Figure 3C shows the custom-built instrument configuration located in Seongbuk-gu, Seoul, Republic of Korea (Korea University, research and development center at 37°35′24.0″N 127°01′36.4″E), used to measure the daytime radiative cooling performance in outdoor surroundings. To minimize the conductive and convective heat transfer, the samples were placed on an insulator (i.e., Styrofoam) and fixed with a wood frame, which was encapsulated by wind shield (i.e., low-density polyethylene [LDPE]), as shown in the left inset image of Figure 3C. In this way, we were able to effectively isolate the radiative cooling performances from the conductive and convective effects, as in previously reported works.  $^{1,4-6,8,9,11-15,17,19-25,34}$  Furthermore, the wood frame was designed to be sufficiently large (900 mm wide and 500 mm deep) to prevent thermal interaction with the sample. Then, the entire setup was tilted 30° toward the south (Figure 3C), ensuring that the samples received sunlight without shadowing during the daytime. The cooling performances of the structured fluids films were measured for two cases: structured fluids coated on (1) a reflective substrate (i.e., a flat Ag mirror) and (2) an absorptive substrate (i.e., Si wafer). The temperature and solar irradiance were logged every 5 s using our custom measuring instruments (right inset image of Figure 3C). In the case of the cooling power measurement, we used a flexible polyimide heater as with the previously reported works (see detailed measuring schematic and methods in Figures S11 and S12A). 13,21,34

Figure 3D profiles the outdoor radiative cooling performance of the structured fluids coated on reflective substrate (i.e., flat Ag mirror) and solar irradiance for 6 h from 12:00 on March 14, 2024. During the daytime, all samples achieved a sub-ambient temperature ( $\sim$ 2 K) with a cooling power of  $\sim$ 40 W/m² as shown in Figure 3E. For example, from 12:00 to 14:00, the average temperature of the ambient air was 304.35 K. At this temperature, the radiative heat exchange ( $P_{rad} - P_{atm}$ ) of R, G, and B structured fluids films was calculated to be 135.7, 135.2, and 135.17 W/m², respectively. In addition, the average solar absorption ( $P_{sun}$ ) was 95.42 W/m² (Figure S12B) and the non-radiative heat transfer ( $P_{non-rad}$ ) was 0 W/m². Therefore, the net cooling power of R, G, and B structured fluids films ( $P_{net}$ ) was calculated to be 40.28, 39.78, and 39.75 W/m², respectively (Figure S12C). However, the cooling power could vary depending on location (i.e., latitude and longitude), as theoretically predicted in Figure S13. In particular, the cooling power of the structured fluids can reach up to  $\sim$ 150 W/m² in hot and arid regions.

In contrast, the structured fluids films with the absorptive substrates (i.e., Si wafer) were able to be heated over 333.15 K due to the high solar absorption, compared to the reflective substrate (Figure S15A). Figure 3F profiles the temperature of the structured fluids coated on Si wafer and solar irradiance for 6 h from 12:00 on June 22, 2022. (see 48-h outdoor experimental results in Figure S14). Regardless of colorization, the structured fluids films effectively cooled the Si wafer by up to 9.5 K under the solar irradiance of 877 W/m<sup>2</sup> (Figure 3F). Based on the experimental data, we can estimate the non-radiative heat transfer coefficient ( $h_{non-rad}$ ) by assuming that the structured fluids films reached the thermal equilibrium (i.e., at the equilibrium temperature). In this case, the  $h_{non-rad}$  was estimated to be 6.61  $W/m^2$  K, considering that the  $P_{net}$  should be 0  $W/m^2$ . From these results, we calculated the cooling power of the structured fluids films coated on the Si wafer (Figure \$15B). In detail, the time-traced radiative and non-radiative heat exchanges were calculated depending on the temperatures of coolers, corresponding to Figure 3F. Subsequently, the  $P_{net}$  was calculated by considering the time-traced  $P_{sun}$ . The cooling performance of the structured fluids coated on an absorptive substrate is more sensitive to solar irradiance, compared to those on a reflective substrate.

#### Article



This is due to the high solar absorptivity of the underlying absorptive substrate. For example, at 12:00, the R, G, and B structured fluids films reduced the thermal load of the Si wafer by 121.8, 84.2, and 78.3 W/m², respectively (Figure S15C). However, under low solar irradiance (i.e., at 18:00), the cooling power (i.e., heat dissipation power) of the R, G, and B structured fluids films was calculated to be 25.18, 23.44, and 21.97 W/m², respectively (Figure S15D). Since the R fluid film was able to reflect the most sunlight (Figures 2C and 2D), it presents the highest cooling power among the three samples. Therefore, we experimentally measured the cooling power of the R as a representative example of the structured fluids on an absorptive substrate (Figure 3G). At high solar irradiation (i.e., 12:00–15:00), the average cooling power was measured to be 124.8 W/m², with an SD of 21.1 W/m². In contrast to the structured fluids on a reflective substrate, the average cooling power decreased to 24.6 W/m², with an SD of 7.23 W/m² at sunset (i.e., 17:00–18:00). The measured cooling powers are consistent with the theoretical predictions across the various surrounding conditions (Figure S15B).

#### **Applications of structured fluids**

Thanks to its exotic soft fluidity, structured fluids can be utilized as vibrant cooling paints, offering direct and practical applications in our lives. As mentioned earlier, these structured fluids can be painted over large areas using a versatile bar coating (see Figure 1D). Figure 4A demonstrates a doctor blade coating of the structured fluids on a 300-  $\times$  160-mm-size plate. Even without the coating machines, structured fluids can be hand-painted onto surfaces as needed, using a plastic tip (Figure 4B) or a simple brush (Figure 4C). This manual application method allows for the creation of complicated patterns and graphics for radiative coolers in an easy-to-craft manner (Figure 4B). In addition, our structured fluids exhibit lower solar absorption, higher solar reflection, and higher thermal emission, compared to commercial paint (Figure \$16). As such, with the same thickness, structured fluids outperform commercial paint in terms of outdoor performance, as evident in the thermal camera image (right-hand image of Figure 4C; temperature difference of 1.8°C) and temperature differences illustrated in Figure 4D. This surface cooling also contributes to lower indoor temperatures, potentially leading to energy savings in air conditioning systems. We compared the surface (Figure 4E) and indoor (Figure 4F) temperatures of two wood boxes (uncoated and coated boxes) in outdoor conditions. As shown in Figure 4E, the boxes (80 mm width, 40 mm depth, and 130 mm height) were placed in the same location in Figure 3C. The coated box presented a 1.2°C lower surface temperature compared to the uncoated box (inset image of Figure 4E). Furthermore, the indoor temperature of the coated box remained consistently 0.5°C lower than the uncoated box for 90 min, as shown in Figure 4F.

Beyond its straightforward usage as a large-scale painting, we can enhance emissivity (i.e., emissivity value of 1.0) by structuring fluids into a thermal PhC. As a proof-of-concept, a two-dimensional (2D) PhC composed of a regular post array with 4  $\times$  4  $\mu m$  in width, 10  $\mu m$  in height, and 12  $\mu m$  in periodicity was fabricated using a versatile flash-assisted nanoimprint process (Figure S17).  $^{51}$  Our results highlight that this PhC emitter can achieve ideal IR emissivity, benefiting from the following synergistic interplay between several modes.

First, radiated electromagnetic waves can escape only along a certain angular range (i.e., escape cone) defined by the refractive index of the material. A PhC can expand this escape cone by the momentum-kicking effect of the grating vector (G(r)) (Figure 5A). 52,53 Second, electromagnetic waves can be confined at the surface of the PhC emitter, giving rise to multiple reflections, also referred to as cavity resonance



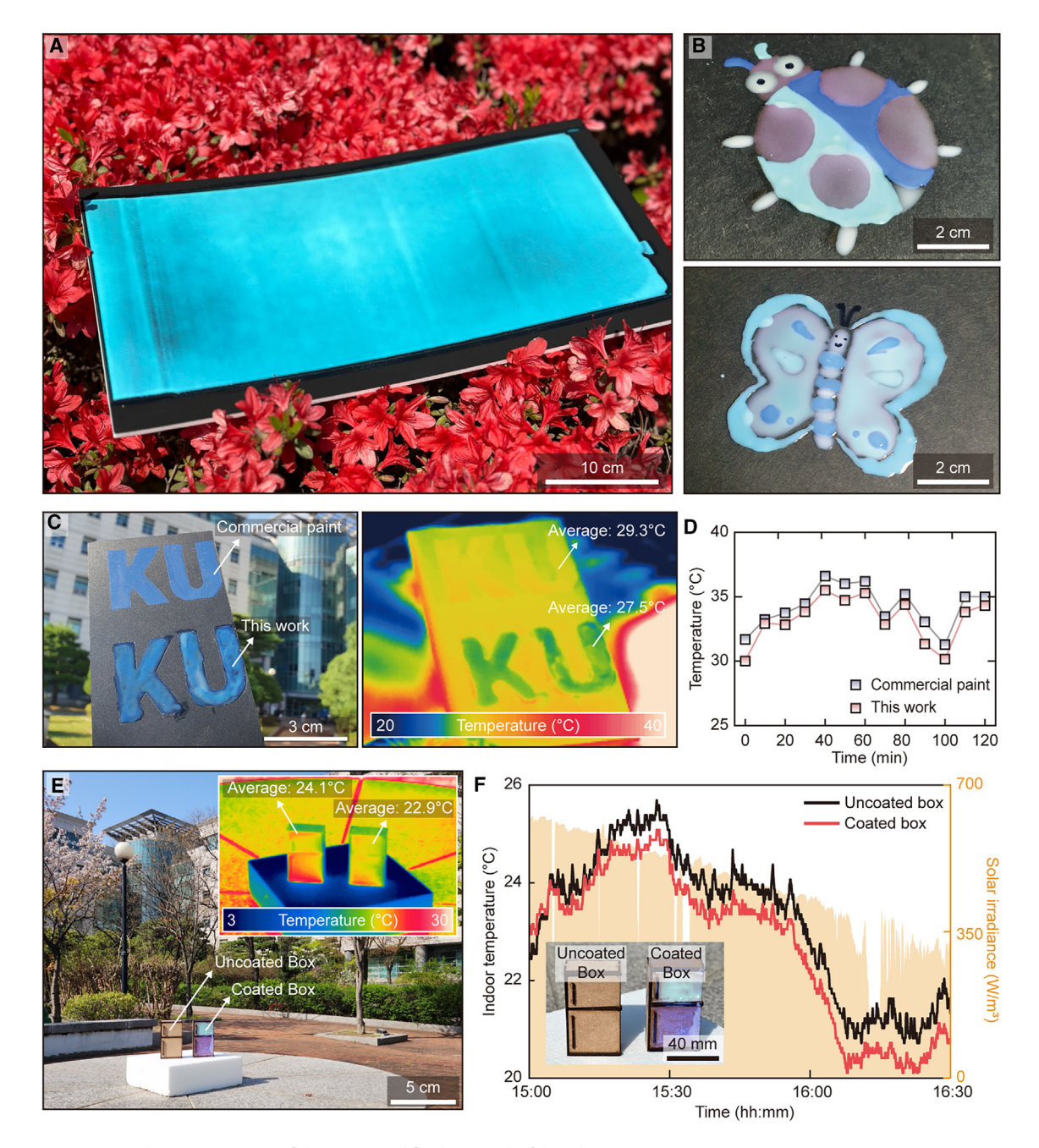


Figure 4. Daytime outdoor experiments of the structured fluids as a colorful cooling paint

- (A) Macroscopic image of the coated and robustly cured structured fluids on a plate (i.e., size of 300  $\times$  160 mm) using a doctor blade.
- (B) Digital camera image of a ladybug (top) and a butterfly (bottom), which were painted with the structured fluids using plastic tips.
- (C) Digital camera image (left) and thermal camera image (right) of the commercial paint and cured structured fluids, written as "KU."
- (D) Time-traced outdoor temperature variations of the samples corresponding to (C) for 2 h.
- (E) Bird's-eye view and thermal camera image (inset) of the uncoated box and coated box with structured fluids. The dimensions of the box are 80, 40, and 130 mm in width, depth, and height, respectively, and the measurement location was the same as in Figure 3C.
- (F) Time-traced temperature variation in the indoor of the 2 boxes was measured on April 7, 2023.

at the wavelength ( $\lambda_{cr}$ ) of 6.25, 7.42, 8.20, 9.66, 10.77, and 11.77  $\mu$ m. This phenomenon enhances absorption and emission across a broad IR range. <sup>54,55</sup> Figure 5B summarizes the modal analysis for both flat (left) and PhC (right) emitters, specifically focusing on the 8.20- $\mu$ m wavelength as a representative example. The counterparts



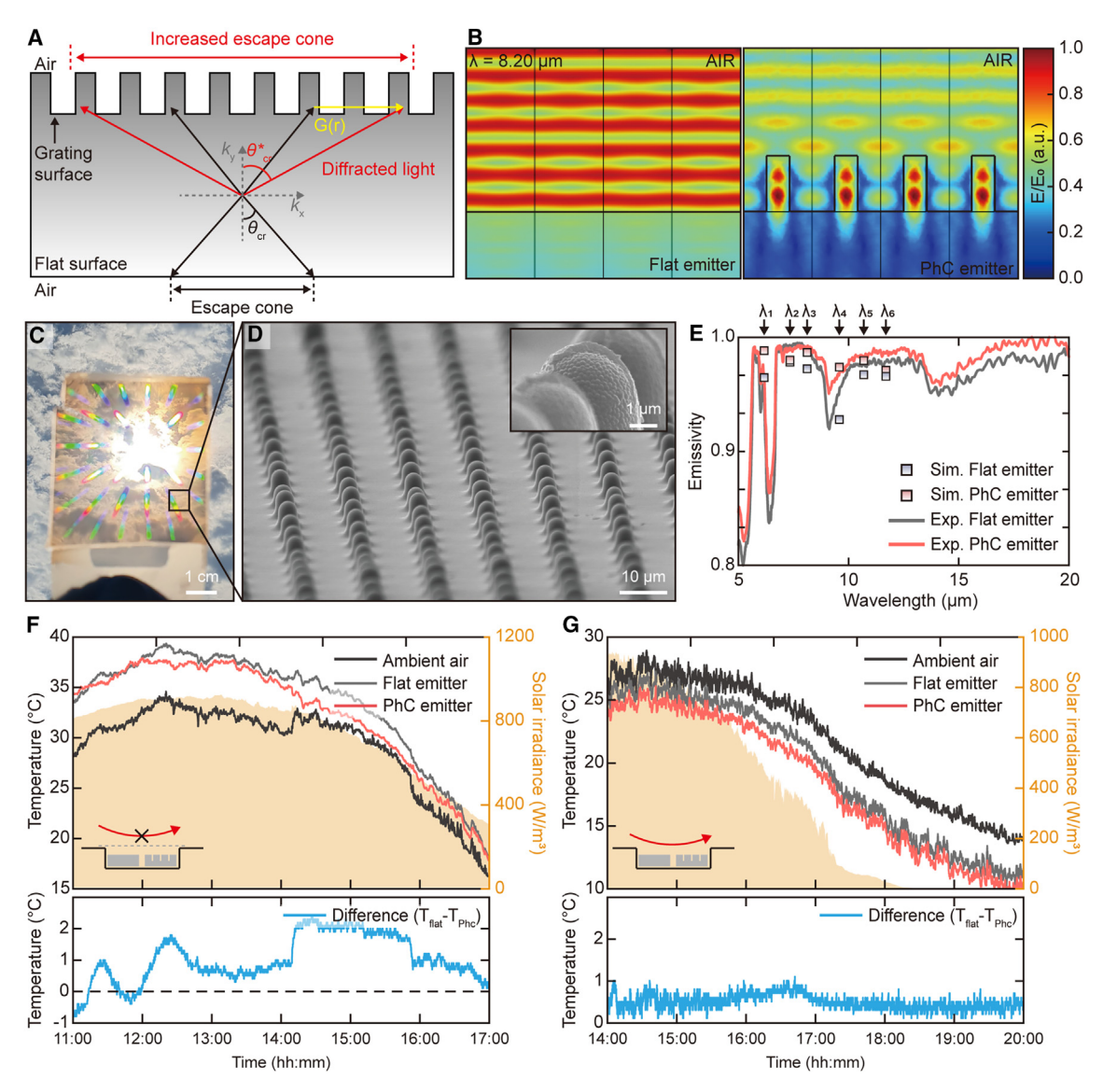


Figure 5. Thermal PhC by soft imprinting of structured fluids

(A) Schematic illustration of the photon escape cone between the air and thermal emitter. The grating surface (top) with the grating vector (G(r)) exhibits an increased photon escape cone compared to the flat surface (bottom).

(B) Simulation results depicting the interaction of electromagnetic waves with the flat (left) and PhC (right) emitters at 8.20  $\mu$ m, corresponding to the cavity resonance wavelength ( $\lambda_{cr}$ ).

(C and D) Digital camera (C) and SEM (D) images of the centimeter-scale PhC thermal emitter. (Inset) Each rectangular post consists of silica nanoparticles randomly dispersed in an acrylate matrix (ETPTA).

(E) Experimentally measured thermal emissivity of the structured fluids films, with flat and PhC emitters in the mid-IR range.

(F and G) Time-traced temperature variation of the structured fluids films (flat and PhC emitters) and solar irradiation with (F) and without (G) the LDPE encapsulation. The temperature differences between the flat and PhC emitters (the temperature of the flat emitter  $[T_{fhc}]$ ) were profiled at bottom. Each measurement was conducted on March 31, 2023 (F) and March 30, 2023 (G), and the data were recorded for 6 h.

at the other wavelengths are included in Figure S18. Third, each cuboid with a periodicity of 12  $\mu$ m can oscillate individually as a polar-dielectric resonator, localizing the surface phonon-polariton mode to the post and exciting a higher mode of the optical phonon (i.e., Fröhlich resonance). <sup>56,57</sup>

Figures 5C and 5D respectively show macroscopic and microscopic SEM images of the centimeter-scale structured fluids film with the nanoimprinted surface (i.e., PhC



emitter). The iridescent colors in Figure 5C illustrate the high macroscopic integrity and uniformity of the PhC emitter. In each post of the PhC emitter, randomly organized silica colloids were visible (inset of Figure 5D). Despite structural imperfections, such as imperfectly defined cylindrical posts, the ensemble effect of the PhC significantly increased emissivity compared to a flat emitter (Figure 5E). Simulation and experimental results both highlighted emissivity enhancement at six different  $\lambda_{cr}$  (black arrows in Figure 5E). As a result, the thermal PhC emitter marked an emissivity value of up to 0.96 in the IR range (i.e., 5–20  $\mu$ m), while the flat emitter showed 0.94 in the same range.

Subsequently, we contrasted the outdoor radiative cooling performance between a flat and thermal PhC emitter at the same location as in Figure 3C. Figures 5F and 5G respectively present the experimental results of freestanding thermal emitters with (Figure 5F) and without (Figure 5G) LDPE encapsulation. Under the encapsulated condition (Figure 5F), both emitters were hotter than the ambient air across the experiments (6 h from 11:00 on March 31, 2023). In this case, the PhC emitter was colder than the flat emitter by  $\sim\!1^\circ\text{C}-2^\circ\text{C}$  for 5 h from 12:00, under the solar irradiance of  $\sim\!800~\text{W/m}^2$ . In contrast to the encapsulated condition, the total radiative cooling performance of the PhC emitter slightly decreased when they were exposed to outdoor environments (Figure 5G). This is because conduction and convection heat exchange are actively involved in the cooling of the emitter. Therefore, both emitters were colder than the ambient air, and the temperature difference between the two emitters dropped to 0.5°C during the 6 h from 14:00 on March 30.

In conclusion, we demonstrate for the first time that, as a reflection-based radiative cooler, randomly dispersed silica colloids in an acrylate matrix (i.e., structured fluids) are suitable materials for reflective colorization, broadband thermal emission, and straightforward usage. Benefiting from the exotic soft fluidity, scalability, and processibility of the materials, structured fluids could paint any on-demand substrate over the meter scale. Their extremely low solar absorption and broadband thermal emission allowed the structured fluids films to achieve sub-ambient (2 K) daytime radiative cooling performance with a cooling power of  $\sim$ 40 W/m<sup>2</sup>. In addition, the structured fluids films can cool an absorptive substrate by as much as 9.5 K with a cooling power of ~120 W/m<sup>2</sup>. Moreover, versatile molding of the structured fluids into the PhCs enables more efficient dissipation of parasitic heat. These thermal PhC emitters exhibited  $\sim$ 1°C -2°C lower temperatures than the flat emitter, and even without LDPE encapsulation, the PhC emitter remained colder by as much as 0.5°C. Above all, since these cooling engineering applications are directly related to indoor cooling and are compatible with current cooling systems, structured fluids can promote energy saving as environmentally friendly and colorful cooling surfaces.

#### **EXPERIMENTAL PROCEDURES**

#### Resource availability

Lead contact

Seungwoo Lee (seungwoo@korea.ac.kr).

#### Materials availability

This study did not generate new unique materials.

#### Data and code availability

The authors declare that the data associated with the study are included in the article and the supplemental information. All other data are available from the lead contact upon reasonable request.

#### **Article**



#### Synthesis of silica colloids

All chemical reagents, including anhydrous ethanol (Sigma-Aldrich,  $\geq$  99.5%), ammonia solution (Sigma-Aldrich, 25%), and tetraethyl orthosilicate (TEOS, Sigma-Aldrich,  $\geq$  99.0%) were used as received. Deionized (DI) water was prepared by using Milli-Q Pure water. Silica colloids were synthesized by a slightly modified solvent-varying method from the Stöber method. The solvent comprised ethanol and DI water, ammonia acted as the catalyst, and TEOS served as the precursor. The ratio of ammonia solution:TEOS:DI water was fixed at 6:8:3, while the ratio of ethanol was varied from 82 to 94, allowing precise control of silica colloid size from 120 to 180 nm. The mixture was stirred for 2 h at 60°C, and after synthesis, the colloids were centrifuged at 1,500 relative centrifugal force for 1 h and washed with ethanol two times.

#### **Fabrication process of structured fluids**

Silica colloid powder was collected by evaporating the colloidal solvent. One gram of silica colloids was re-dispersed in pure ethanol. ETPTA (Sigma-Aldrich, average Mn  $\sim$ 428) was added to the silica colloids, varying the vol% from 15 to 30. After mixing, ethanol was evaporated at 65°C, and finally, 1 wt % Darocur 1173 was added for UV curing.

#### Ag layer deposition on the structured fluids

A 200-nm Ag layer is deposited on cured structured fluids films using a thermal evaporation system (DKTE01-04, DaeKI HI-TECH). During deposition, a thickness of the Ag was monitored by a quartz crystal sensor.

#### Optical setup for measuring absorptivity/emissivity of structured fluids films

Reflectance and transmittance were measured using Fourier transform IR spectroscopy (FTIR, INVENIO-X, Bruker) with reflectance accessories, including polytetra-fluoroethylene-coated integrating sphere for visible frequency, Au-coated integrating sphere for IR frequency, and angle adjustment accessory for quantified reflected lights for each angle. Emissivity was calculated from reflectivity and transmissivity. All measurements were carried out using the computer program OPUS.

#### Optical setup for measuring angle-dependent reflection spectra

The angle-resolved reflection spectra were quantified with FTIR spectroscopy (INVENIO-X) equipped with an angle adjustment accessory. The incident light angle ( $\phi$ ) was fixed at 13°, while the detecting sensor angle ( $\theta$ ) was varied from 21° to 69°, with 4° intervals.

#### Experiments on cooling performance of structured fluids films

Outdoor experiments for verifying the cooling effect were carried out in front of the KU research and development center, Korea University, Seoul, Korea (37°35′24.0″N 127°01′36.4″E). A custom setup, composed of wood frame, Styrofoam, LDPE, thermometer (TM-947SD), K-type thermocouple (ST-50), solar power meter (SPM-1116SD), hygrometer (AM-4237SD), polyimide film insulated flexible heaters (Omega KHLVA-101/1-P), power source (Keithley dual sourcemeter, 2230-30-1), and laptop (LG gram), were used to quantify the cooling performance of the samples as shown in Figure 3. Thermocouples were attached to the backside of the samples, and the samples were placed in an encapsulated chamber. Data were logged by laptop using the proportional-integral-derivative control system.





#### **Experiments on paintings**

For large-scale painting experiments, 30 g silica colloids were used to fabricate structured fluids. Painting was done using a brush (Rubens 590, 0 size), plastic tips, or a lab coating machine (Rotec, CV-400) for sizes over  $300 \times 160$  mm. Painted structured fluids were cured using a UV lamp with a UVB wavelength range.

#### **Experiments on imprinting**

Conventional soft lithography was used to fabricate a thermal PhC emitter. Polyethylene terephthalate (PET, 300  $\mu m$  thickness) and SU-8 2007 were used to manufacture the master mold. After the conventional photolithography process, structured fluids were poured onto the PET master mold and cured by a UV lamp. The 2D array patterns were obtained by carefully peeling off the PET substrate.

#### **Experiments on cooling performance of flat and PhC emitters**

To verify the cooling performance of the PhC emitters, experiments were conducted using the same instruments as in the experiment in Figure 3C, except for the heater, power source, and laptop. Two cases were conducted: (1) cooling performance of freestanding films with LDPE encapsulation, and (2) cooling performance of freestanding films without LDPE encapsulation. Thermocouples were attached to the backside of each sample, and the samples were placed on Styrofoam. Data (i.e., temperatures and solar irradiation) were logged by the thermometer and solar power meter.

#### SUPPLEMENTAL INFORMATION

Supplemental information can be found online at https://doi.org/10.1016/j.xcrp. 2024.102068.

#### **ACKNOWLEDGMENTS**

This work was supported by the National Research Foundation (NRF) grant (NRF-2022M3H4A1A02074314 and NRF-RS-2023-00272363), the Samsung Research Funding & Incubation Center for Future Technology grant (SRFC-MA2301-02), the KIST Institutional Program (project no. 2V09840-23-P023), and a Korea University grant. This material was partially based upon work supported by the National Science Foundation under grant no. ECCS-2146577 (to A.P.R.).

#### **AUTHOR CONTRIBUTIONS**

H.H.K. and S.L. conceived the original idea. H.H.K., S.K., and E.I. synthesized the colloids. H.H.K. and S.K. assembled them, developed the structured fluids, and painted them onto surfaces as needed. H.H.K. theoretically and experimentally analyzed the spectral emissivity and absorptivity of the structured fluids and conducted the outdoor experiments. J.L. and E.I. theoretically analyzed the diffusive light scattering of the structured fluids. S.L. and A.P.R. supervised the project. The manuscript was mainly written by H.H.K., A.P.R., and S.L., with the contributions of all authors.

#### **DECLARATION OF INTERESTS**

The authors declare no competing interests.

Received: February 21, 2024 Revised: May 16, 2024 Accepted: June 6, 2024 Published: June 28, 2024

#### **Article**



#### **REFERENCES**

- Raman, A.P., Anoma, M.A., Zhu, L., Rephaeli, E., and Fan, S. (2014). Passive radiative cooling below ambient air temperature under direct sunlight. Nature 515, 540–544. https://doi.org/ 10.1038/nature13883.
- Munday, J.N. (2019). Tackling Climate Change through Radiative Cooling. Joule 3, 2057–2060. https://doi.org/10.1016/j.joule.2019.07.010.
- Zhu, L., Raman, A., and Fan, S. (2013). Color-preserving daytime radiative cooling. Appl. Phys. Lett. 103, 223902. https://doi.org/10. 1063/1.4835995.
- Lee, G.J., Kim, Y.J., Kim, H.M., Yoo, Y.J., and Song, Y.M. (2018). Colored, Daytime Radiative Coolers with Thin-Film Resonators for Aesthetic Purposes. Adv. Opt. Mater. 6, 1800707. https://doi.org/10.1002/adom. 201800707.
- Li, W., Shi, Y., Chen, Z., and Fan, S. (2018). Photonic thermal management of coloured objects. Nat. Commun. 9, 4240. https://doi. org/10.1038/s41467-018-06535-0.
- Luo, H., Li, Q., Du, K., Xu, Z., Zhu, H., Liu, D., Cai, L., Ghosh, P., and Qiu, M. (2019). An ultrathin colored textile with simultaneous solar and passive heating abilities. Nano Energy 65, 103998. https://doi.org/10.1016/j.nanoen. 2019.103998.
- 7. Cai, L., Peng, Y., Xu, J., Zhou, C., Zhou, C., Wu, P., Lin, D., Fan, S., and Cui, Y. (2019). Temperature Regulation in Colored Infrared-Transparent Polyethylene Textiles. Joule 3, 1478–1486. https://doi.org/10.1016/j.joule. 2019.03.015.
- Kim, H.H., Im, E., and Lee, S. (2020). Colloidal Photonic Assemblies for Colorful Radiative Cooling. Langmuir 36, 6589–6596. https://doi. org/10.1021/acs.langmuir.0c00051.
- Chen, Y., Mandal, J., Li, W., Smith-Washington, A., Tsai, C.C., Huang, W., Shrestha, S., Yu, N., Han, R.P.S., Cao, A., and Yang, Y. (2020). Colored and paintable bilayer coatings with high solar-infrared reflectance for efficient cooling. Sci. Adv. 6, eaaz5413. https://doi.org/ 10.1126/sciadv.aaz5413.
- Yalçın, R.A., Blandre, E., Joulain, K., and Drévillon, J. (2020). Colored Radiative Cooling Coatings with Nanoparticles. ACS Photonics 7, 1312–1322. https://doi.org/10.1021/ acsphotonics.0c00513.
- Ding, Z., Pattelli, L., Xu, H., Sun, W., Li, X., Pan, L., Zhao, J., Wang, C., Zhang, X., Song, Y., et al. (2022). Iridescent Daytime Radiative Cooling with No Absorption Peaks in the Visible Range. Small 18, 2202400. https://doi.org/10.1002/ smll.202202400.
- Yu, S., Zhang, Q., Wang, Y., Lv, Y., and Ma, R. (2022). Photonic-Structure Colored Radiative Coolers for Daytime Subambient Cooling. Nano Lett. 22, 4925–4932. https://doi.org/10. 1021/acs.nanolett.2c01570.
- Jin, S., Xiao, M., Zhang, W., Wang, B., and Zhao, C. (2022). Daytime Sub-Ambient Radiative Cooling with Vivid Structural Colors Mediated by Coupled Nanocavities. ACS Appl. Mater. Interfaces 14, 54676–54687. https://doi. org/10.1021/acsami.2c15573.

- Zhu, W., Droguet, B., Shen, Q., Zhang, Y., Parton, T.G., Shan, X., Parker, R.M., De Volder, M.F.L., Deng, T., Vignolini, S., and Li, T. (2022). Structurally Colored Radiative Cooling Cellulosic Films. Adv. Sci. 9, 2202061. https:// doi.org/10.1002/advs.202202061.
- Son, S., Chae, D., Lim, H., Ha, J., Park, J., Ju, S., Park, J., Kim, W., and Lee, H. (2022). Temperature-Sensitive Colored Radiative Cooling Materials with Efficient Cooling Performance. Adv. Eng. Mater. 25, 2201254. https://doi.org/10.1002/adem.202201254.
- Jeon, S., Son, S., Min, S., Park, H., Lee, H., and Shin, J. (2022). Daylong Sub-Ambient Radiative Cooling with Full-Color Exterior Based on Thermal Radiation and Solar Decoupling. Adv. Opt. Mater. 11, 2202129. https://doi.org/10. 1002/adom.202202129.
- Li, X., Xu, H., Yang, Y., Li, F., Ramakrishna, S., Yu, J., Ji, D., and Qin, X. (2023). Selective spectral absorption of nanofibers for colorpreserving daytime radiative cooling. Mater. Horiz. 10, 2487–2495. https://doi.org/10.1039/ DAMM003010.
- Min, S., Jeon, S., Yun, K., and Shin, J. (2022). All-Color Sub-ambient Radiative Cooling Based on Photoluminescence. ACS Photonics 9, 1196–1205. https://doi.org/10.1021/acsphotonics.1c01648.
- Ao, X., Li, B., Zhao, B., Hu, M., Ren, H., Yang, H., Liu, J., Cao, J., Feng, J., Yang, Y., et al. (2022). Self-adaptive integration of photothermal and radiative coolingfor continuous energy harvesting from the sun and outer space. Proc. Natl. Acad. Sci. USA 119, e2120557119. https:// doi.org/10.1073/pnas.2120557119.
- Zhao, X., Aili, A., Zhao, D., Xu, D., Yin, X., and Yang, R. (2022). Dynamic glazing with switchable solar reflectance for radiative cooling and solar heating. Cell Rep. Phys. Sci. 3, 100853. https://doi.org/10.1016/j.xcrp.2022. 100853
- 21. Lin, K., Chen, S., Zeng, Y., Ho, T.C., Zhu, Y., Wang, X., Liu, F., Huang, B., Chao, C.Y.-H., Wang, Z., and Tso, C.Y. (2023). Hierarchically structured passive radiative cooling ceramic with high solar reflectivity. Science 382, 691–697. https://doi.org/10.1126/science.adi/1725
- Zhao, X., Li, T., Xie, H., Liu, H., Wang, L., Qu, Y., Li, S.C., Liu, S., Brozena, A.H., Yu, Z., et al. (2023). A solution-processed radiative cooling glass. Science 382, 684–691. https://doi.org/10. 1126/science.adi2224.
- Zeng, S., Pian, S., Su, M., Wang, Z., Wu, M., Liu, X., Chen, M., Xiang, Y., Wu, J., Zhang, M., et al. (2021). Hierarchical-morphology metafabric for scalable passive daytime radiative cooling. Science 373, 692–696. https://doi.org/10.1126/ science.abi5484.
- Zhu, B., Li, W., Zhang, Q., Li, D., Liu, X., Wang, Y., Xu, N., Wu, Z., Li, J., Li, X., et al. (2021). Subambient daytime radiative cooling textile based on nanoprocessed silk. Nat. Nanotechnol. 16, 1342–1348. https://doi.org/10.1038/s41565-021-00987-0.
- 25. Li, D., Liu, X., Li, W., Lin, Z., Zhu, B., Li, Z., Li, J., Li, B., Fan, S., Xie, J., and Zhu, J. (2021). Scalable

- and hierarchically designed polymer film as a selective thermal emitter for high-performance all-day radiative cooling. Nat. Nanotechnol. 16, 153–158. https://doi.org/10.1038/s41565-020-00800-4.
- 26. Witten, T.A., and Pincus, P.A. (2004). Structured Fluids: Polymers, Colloids, Surfactants (Oxford University Press).
- Witten, T.A. (1990). Structured fluids. Phys. Today 43, 21–28. https://doi.org/10.1063/1. 881249.
- García, P.D., Sapienza, R., Blanco, A., and López, C. (2007). Photonic Glass: A Novel Random Material for Light. Adv. Mater. 19, 2497–2602. https://doi.org/10.1002/adma. 2006/02476
- García, P.D., Sapienza, R., and López, C. (2010). Photonic glasses: a step beyond white paint. Adv. Mater. 22, 12–19. https://doi.org/10.1002/adma.200900827.
- Magkiriadou, S., Park, J.-G., Kim, Y.-S., and Manoharan, V.N. (2014). Absence of red structural color in photonic glasses, bird feathers, and certain beetles. Phy. Rev. E. 90, 062302. https://doi.org/10.1103/PhysRevE.90. 062302.
- Shang, G., Maiwald, L., Renner, H., Jalas, D., Dosta, M., Heinrich, S., Petrov, A., and Eich, M. (2018). Photonic glass for high contrast structural color. Sci. Rep. 8, 7804. https://doi. org/10.1038/s41598-018-26119-8.
- Jacucci, G., Vignolini, S., and Schertel, L. (2020). The limitations of extending nature's color palette incorrelated, disordered systems. Proc. Natl. Acad. Sci. USA 117, 23345–23349. https://doi.org/10.1073/pnas.2010486117.
- Liu, T., Liu, T., Gao, F., Glotzer, S.C., and Solomon, M.J. (2022). Structural Color Spectral Response of Dense Structures of Discoidal Particles Generated by Evaporative Assembly. J. Phys. Chem. B 126, 1315–1324. https://doi. org/10.1021/acs.jpcb.1c10015.
- Li, T., Zhai, Y., He, S., Gan, W., Wei, Z., Heidarinejad, M., Dalgo, D., Mi, R., Zhao, X., Song, J., et al. (2019). A radiative cooling structural material. Science 364, 760–763. https://doi.org/10.1126/science.aau9101.
- Zhou, L., Song, H., Liang, J., Singer, M., Zhou, M., Stegenburgs, E., Zhang, N., Xu, C., Ng, T., Yu, Z., et al. (2019). A polydimethylsiloxanecoated metal structure for all-day radiative cooling. Nat. Sustain. 2, 718–724. https://doi. org/10.1038/s41893-019-0348-5.
- Xie, W., Xiao, C., Sun, Y., Fan, Y., Zhao, B., Zhang, D., Fan, T., and Zhou, H. (2023). Flexible Photonic Radiative Cooling Films: Fundamentals, Fabrication and Applications. Adv. Funct. Mater. 33, 2305734. https://doi. org/10.1002/adfm.202305734.
- Ha, H.-J., Kwon, Y.H., Kim, J.Y., and Lee, S.Y. (2011). A self-standing, UV-cured polymer networks-reinforced plastic crystal composite electrolyte for a lithium-ion battery. Electrochim. Acta 57, 40–45. https://doi.org/ 10.1016/j.electacta.2011.03.101.
- 38. Gou, Y., Cheng, J., Liu, L., and Tan, Z. (2021). Grains boundary networking interconnection



## Cell Reports Physical Science Article

- design for robust flexible perovskite solar cell. Mater. Lett. 292, 129559. https://doi.org/10.1016/j.matlet.2021.129559.
- Fang, Y., Ni, Y., Leo, S.-Y., Taylor, C., Basile, V., and Jiang, P. (2015). Reconfigurable photonic crystals enabled by pressure-responsive shape-memory polymers. Nat. Commun. 6, 7416. https://doi.org/10.1038/ncomms8416.
- Whimore, P.M., and Colaluca, V.G. (1995). The Natural and Accelerated Aging of an Acrylic Artists' Medium. Stud. Conserv. 40, 51–64. https://doi.org/10.2307/1506611.
- Weiss, K.D. (1997). Paint and coatings: A mature industry in transition. Prog. Polym. Sci. 22, 203–245. https://doi.org/10.1016/S0079-6700(96)00019-6.
- Jiang, P., and McFarland, M.J. (2004). Large-Scale Fabrication of Wafer-Size Colloidal Crystals, Macroporous Polymers and Nanocomposites by Spin-Coating. J. Am. Chem. Soc. 126, 13778–13786. https://doi.org/ 10.1021/ja0470923.
- Kim, S.-H., Jeon, S.-J., Yi, G.-R., Heo, C.-J., Choi, J.-H., and Yang, S.-M. (2008). Optofluidic Assembly of Colloidal Photonic Crystals with Controlled Sizes, Shapes, and Structures. Adv. Mater. 20, 1649–1655. https://doi.org/10.1002/ adma.200703022.
- Cai, C.-Y., Lin, K.-Y.A., Chen, Y.-C., and Yang, H. (2016). Macroporous photonic crystal-based anti-ultraviolet and anti-near-infrared materials by doctor blade coating. Appl. Phys. Lett. 108, 071906. https://doi.org/10.1063/1.4941729.
- 45. Zhao, Y., Xie, Z., Gu, H., Jin, L., Zhao, X., Wang, B., and Gu, Z. (2012). Multifunctional photonic crystal barcodes from microfluidics. NPG Asia

- Mater. 4, 25. https://doi.org/10.1038/am. 2012.46.
- Yang, H., and Jiang, P. (2010). Large-Scale Colloidal Self-Assembly by Doctor Blade Coating. Langmuir 26, 13173–13182. https:// doi.org/10.1021/la101721v.
- 47. Liu, X., Liu, J., Wei, B., Yang, D., Luo, L., Ma, D., and Huang, S. (2023). Bio-Inspired Highly Brilliant Structural Colors and Derived Photonic Superstructures for Information Encryption and Fluorescence Enhancement. Adv. Sci. 10, 2302240. https://doi.org/10.1002/advs. 202302240.
- Zhu, L., Raman, A.P., and Fan, S. (2015). Radiative cooling of solar absorbers using a visibly transparent photonic crystal thermal blackbody. Proc. Natl. Acad. Sci. USA 112, 12282–12287. https://doi.org/10.1073/pnas. 1509453112.
- Böer, K.W., and Pohl, U.W. (2023).
   Semiconductor Physics, 2nd ed., Part IV.
   Photons (Springer cham). https://doi.org/10. 1007/978-3-031-18286-0.
- Wen, J., Chen, X., Zhu, Z., Zhu, Y., Luo, H., Wang, Y., Liu, Y., Wang, H., Yuan, W., Zhang, Y., et al. (2023). Thin film-based colorful radiative cooler using diffuse reflection for color display. PhotoniX 4, 25. https://doi.org/10.1186/ s43074-023-00104-5.
- 51. Zhou, J., Chen, T.G., Tsurimaki, Y., Hajj-Ahmad, A., Fan, L., Peng, Y., Xu, R., Wu, Y., Assawaworrarit, S., Fan, S., et al. (2023). Angle-selective thermal emitter for directional radiative cooling and heating. Joule 7, 2830–2844. https://doi.org/10.1016/j.joule.2023.

- Schnitzer, I., Yablonovitch, E., Caneau, C., Gmitter, T.J., and Scherer, A. (1993). 30% external quantum efficiency from surface textured, thin-film light-emitting diodes. Appl. Phys. Lett. 63, 2174–2176. https://doi.org/10. 1063/1.110575.
- Lim, Y., Kang, B., Hong, S.J., Son, H., Im, E., Bang, J., and Lee, S. (2021). A Field Guide to Azopolymeric Optical Fourier Surfaces and Augmented Reality. Adv. Funct. Mater. 31, 2104105. https://doi.org/10.1002/adfm. 202104105.
- Chen, Y.-B., and Zhang, Z.M. (2007). Design of tungsten complex gratings for thermophotovoltaic radiators. Opt Commun. 269, 411–417. https://doi.org/10.1016/j. optcom.2006.08.040.
- Song, J., Seo, J., Han, J., Lee, J., and Lee, B.J. (2020). Ultrahigh emissivity of gratingpatterned PDMS film from 8 to 13 <i>p
   p wavelength regime. Appl. Phys. Lett. 117, 094101. https://doi.org/10.1063/5. 0017838.
- Zhai, Y., Ma, Y., David, S.N., Zhao, D., Lou, R., Tan, G., Yang, R., and Yin, X. (2017). Scalable-manufactured randomized glass-polymer hybrid metamaterialfor daytime radiative cooling. Science 355, 1062–1066. https://doi. org/10.1126/science.aai7899.
- Jaramillo-Fernandez, J., Whitworth, G.L., Pariente, J.A., Blanco, A., Garcia, P.D., Lopez, C., and Sotomayor-Torres, C.M. (2019). A Self-Assembled 2D Thermofunctional Material for Radiative Cooling. Small 15, 1905290. https://doi.org/10.1002/smll. 201905290.